THE JOURNAL OF PHYSICAL CHEMISTRY LETTERS
A JOURNAL OF THE AMERICAN CHEMICAL SOCIETY

pubs.acs.org/JPCL

Letter

Metal Halide Scaffolded Assemblies of Organic Molecules with Enhanced Emission and Room Temperature Phosphorescence

Maya Chaaban, Azza Ben-Akacha, Michael Worku, Sujin Lee, Jennifer Neu, Xinsong Lin, J. S. Raaj Vellore Winfred, Cordell J. Delzer, Jason P. Hayward, Mao-Hua Du, Theo Siegrist, and Biwu Ma*

Cite This: *J. Phys. Chem. Lett.* 2021, 12, 8229–8236

Read Online

ACCESS | Metrics & More | Article Recommendations | Supporting Information

ABSTRACT: Ionically bonded organic metal halide hybrids have emerged as versatile multicomponent material systems exhibiting unique and useful properties. The unlimited combinations of organic cations and metal halides lead to the tremendous structural diversity of this class of materials, which could unlock many undiscovered properties of both organic cations and metal halides. Here we report the synthesis and characterization of a series benzoquinolinium (BZQ) metal halides with a general formula $(BZQ)Pb_2X_5$ (X = Cl, Br), in which metal halides form a unique two-dimensional (2D) structure. These BZQ metal halides are found to exhibit enhanced photoluminescence and stability as compared to the pristine BZQ halides, due to the scaffolding effects of 2D metal halides. Optical characterizations and theoretical calculations reveal that BZQ^+ cations are responsible for the emissions in these hybrid materials. Changing the halide from Cl to Br introduces heavy atom effects, resulting in yellow room temperature phosphorescence (RTP) from BZQ^+ cations.

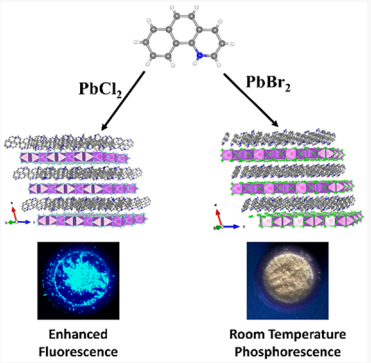

Solid-state organic chromophores have applications in various fields, including photoswitches,[1] sensing,[2] electro-optical modulators,[3] and light emitting diodes (LEDs).[4] The optical properties of organic chromophores, such as emission color and photoluminescence quantum efficiency (PLQE), are controlled by several factors, including their molecular structures and supramolecular modes of assembly and aggregation behaviors.[5−7] To date, numerous strategies have been developed to effectively control the molecular interactions of solid-state organic chromophores to achieve desired optical properties, such as polymorphism[8,9] and cocrystallization.[10] However, the design of reliable approaches that employ molecular interactions in regulating the properties of organic chromophores, also known as crystal engineering, remains a challenging task.[5] Room temperature phosphorescence (RTP) is among various optical properties that can be realized through effective crystal engineering.[11−14] For instance, crystal engineering could promote strong intermolecular interactions in a well-packed structures, which restrict the molecular motions and suppress the nonradiative decays from the triplet state, hence achieving RTP.[14]

Organic metal halide hybrids consisting of organic cations and metal halide anions have received significant attention due to their structure diversity, unique photophysical properties, and wide range of applications.[15−19] Single crystals with different dimensionalities at the molecular level have been developed by carefully choosing the organic cations and metal halides, as well as controlling the synthetic conditions.[20−34] In most of these hybrid materials developed to date, organic cations with wide-bandgap are used to template the assemblies of metal halides without contributing directly to their photophysical properties.[35−37] Recently, photoactive organic cations have been used to develop organic metal halide hybrids with emissions from both organic cations and metal halides, or solely from organic cations.[38−41] The cocrystallization of organic cations with metal halides could enable the manipulation of their photophysical properties by affecting their packing modes and intermolecular interactions. For instance, protonated enrofloxacin exhibited higher PLQE and smaller Stokes shift when it was cocrystallized with $SnCl_6^{2-}$, as compared with other metal halides ($Pb_2Cl_6^{2-}$ to $Bi_2Cl_{10}^{4-}$), due to stronger inter- and intramolecular interactions.[40] In addition, controlling the composition of metal halides could also affect the properties of organic cations by introducing heavy atom effects. For instance, the afterglow properties of tetraphenyl phosphonium zinc halides ($TPPZnX_4$) show strong dependence on the halide composition and $TPPZnBr_4$ exhibits stronger phosphorescence with shorter afterglow than $TPPZnCl_4$.[42]

Received: July 20, 2021
Accepted: August 17, 2021
Published: August 23, 2021

https://doi.org/10.1021/acs.jpclett.1c02354
J. Phys. Chem. Lett. 2021, 12, 8229–8236

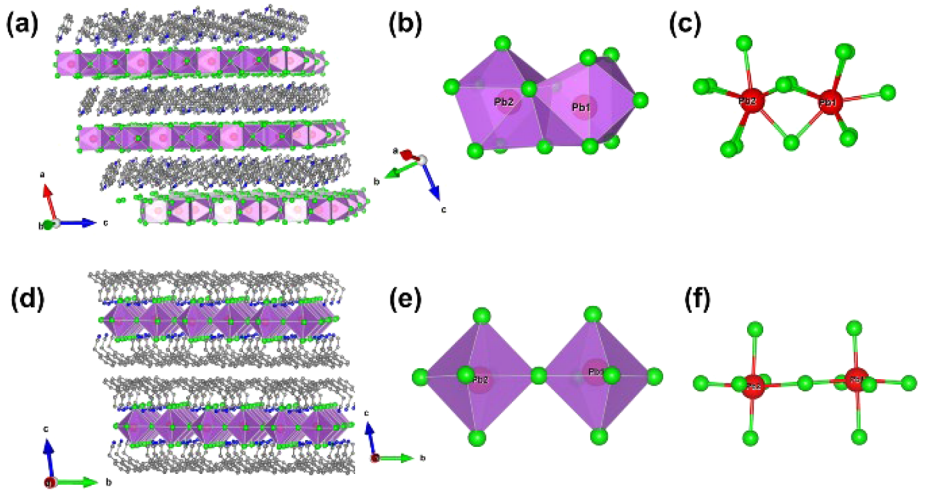

Figure 1. (a) View of the single crystal structure of $(BZQ)Pb_2Br_5$. (b) View of face-sharing decahedra in $(BZQ)Pb_2Br_5$. (c) Ball-and-stick model of an individual the face-sharing decahedra in $(BZQ)Pb_2Br_5$. (d) View of the single crystal structure of a conventional layered 2D A_2PbBr_4 (A = phenylethylammonium). (e) View of corner-sharing octahedra in A_2PbBr_4. (f) Ball-and-stick model of the corner-sharing octahedra in A_2PbBr_4 (Pb, red; Br, green; N, blue; C, gray; hydrogen atoms are omitted for clarity).

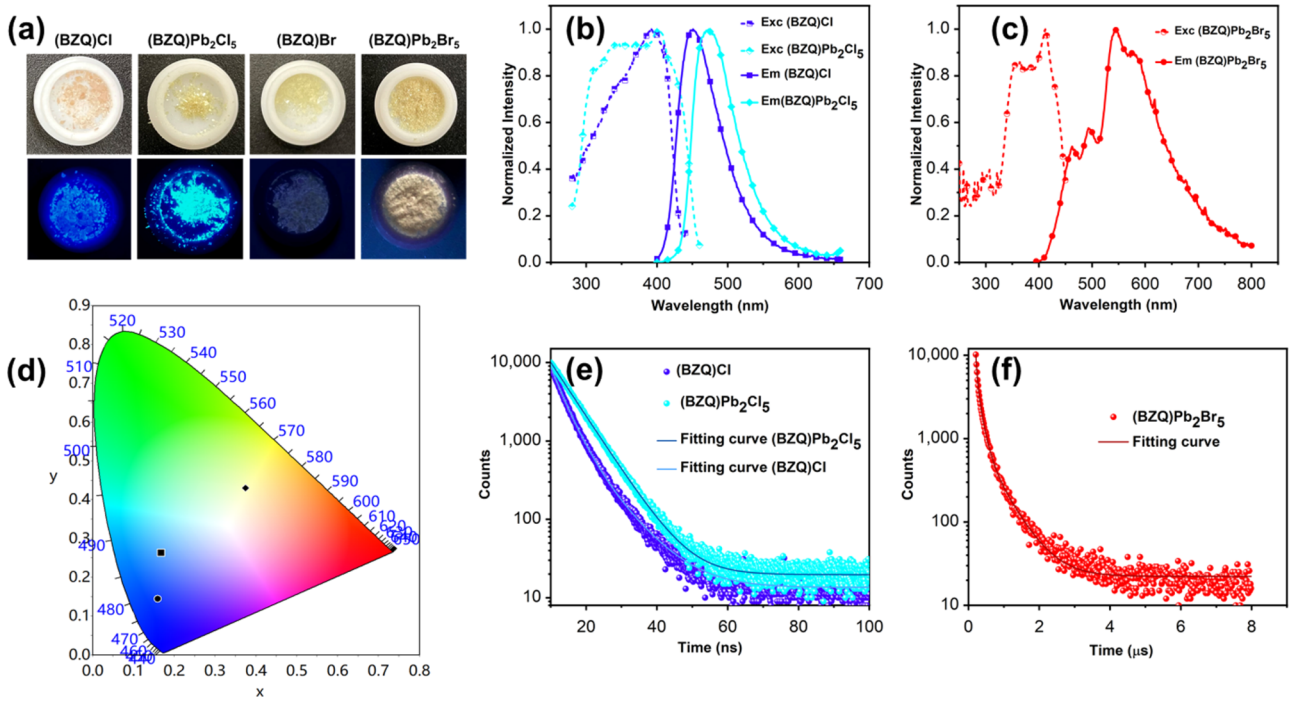

Figure 2. (a) Images showing (BZQ)Cl, $(BZQ)Pb_2Cl_5$, (BZQ)Br, and $(BZQ)Pb_2Br_5$ under ambient and UV light (365 nm). Steady state emission spectra of (b) (BZQ)Cl and $(BZQ)Pb_2Cl_5$ and (c) $(BZQ)Pb_2Br_5$. (d) CIE chromaticity coordinates of the emissions from (BZQ)Cl (circle), $(BZQ)Pb_2Cl_5$ (square), and $(BZQ)Pb_2Br_5$ (rhombus). Emission decay curves of (e) (BZQ)Cl and $(BZQ)Pb_2Cl_5$ and (f) $(BZQ)Pb_2Br_5$.

Here we report two 2D organic metal halide hybrids $(BZQ)Pb_2X_5$ (X = Cl, Br) prepared by cocrystallizing protonated BZQ^+ ($C_{13}NH_{10}^+$) cations with lead halides (PbX_2). BZQ^+ cations were found to be responsible for the emissions of these materials, while the inorganic layers ($Pb_2X_5^-$) act as wide-bandgap scaffold for the organic cations, affecting their assemblies and photophysical properties. $(BZQ)Pb_2Cl_5$ is found to exhibit enhanced blue emission at room temperature as compared to the organic salt (BZQ)Cl, while $(BZQ)Pb_2Br_5$ exhibits yellow RTP due to heavy atom effects of Br. Furthermore, white emission from $(BZQ)Pb_2Cl_5$ is achieved at 77 K due to simultaneous fluorescent and phosphorescent emissions from BZQ^+. In addition to photophysical properties, these solid-state organic metal halide hybrids exhibited significantly better thermal and environmental stability than pure organic halide salts.

Benzoquinolinium metal halides $(BZQ)Pb_2X_5$ (X = Cl, Br) were synthesized by reacting benzo[*h*]quinoline with lead halides (PbX_2) in water in the presence of appropriate acids at 100 °C. Small yellowish plate crystals were obtained upon cooling the reaction mixture. Details of the synthesis can be found in the Supporting Information (Figure S1a). The crystal structures of $(BZQ)Pb_2X_5$ (X = Cl, Br) were determined using single crystal X-ray diffraction (SCXRD). It is found that they

https://doi.org/10.1021/acs.jpclett.1c02354
J. Phys. Chem. Lett. 2021, 12, 8229−8236

Table 1. Summary of the Photophysical Properties of (BZQ)Cl, (BZQ)Pb_2Cl_5, (BZQ)Br, and (BZQ)Pb_2Br_5 at Room Temperature and 77 K

		lifetime				
	emission, λ_{max} (nm)	fluo (ns)	phos (ms)	Φ_{PL} (%)	k_r (s^{-1})	k_{nr} (s^{-1})
(BZQ)Cl	450 (445, 512, 540)[a]	5.0 (8.8)[a]	120[a]	8	0.16×10^8	1.8×10^8
(BZQ)Pb_2Cl_5	470 (450, 480, 524, 572)[a]	6.3 (7.53)[a]	150[a]	18	0.29×10^8	1.3×10^8
(BZQ)Br	N/A (512)[a]	N/A	5.0×10^{-4} [a]	N/A	N/A	N/A
(BZQ)Pb_2Br_5	550 (534, 582)[a]	N/A	2.3×10^{-4} (5.3×10^{-4})[a]	2	0.9×10^5	42×10^5

[a]Measured at 77 K. The radiative and nonradiative decays were calculated using these equations: $k_r = \Phi/\tau$, $k_{nr} = (1 - \Phi)/\tau$.

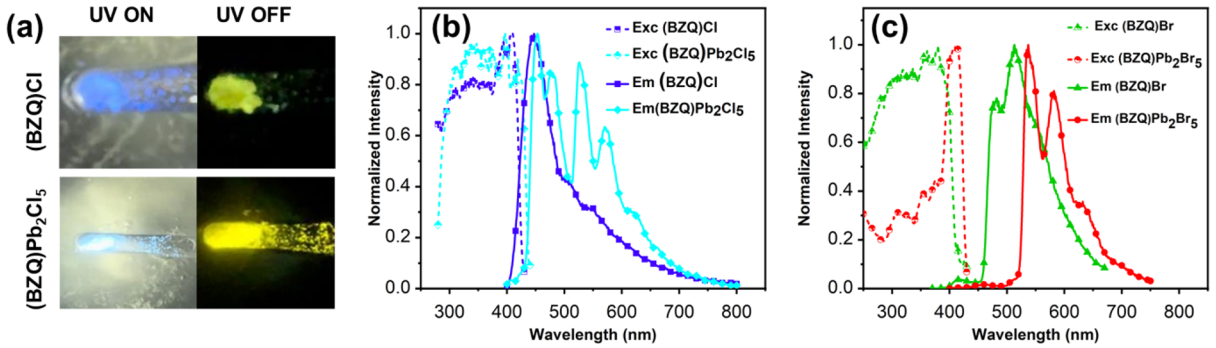

Figure 3. (a) Images showing the prompt and delayed emissions of (BZQ)Cl and (BZQ)Pb_2Cl_5 at 77 K. Steady state emission spectra at 77 K of (b) (BZQ)Cl and (BZQ)Pb_2Cl_5 and (c) (BZQ)Br and (BZQ)Pb_2Br_5.

are isostructural and crystallize in the monoclinic space group $P2_1/c$ (Table S1). As shown in Figure 1a and S1, the structures are composed of 2D anionic sheets of $[Pb_2X_5]^-$ separated and balanced by arrays of BZQ^+ cations. This new 2D structure is very different from the conventional corner-shared 2D metal halide structure found in layered 2D perovskites with a general formula of A_2PbX_4.[43,44] In this unique 2D structure described for the first time, Pb atoms are coordinated to eight halides to form face-sharing decahedra, unlike the case of conventional 2D, where the Pb atoms coordinate to six halides to form corner-sharing octahedra (Figure 1 and Figure S2). The Pb−X bond lengths range from 2.712 to 3.273 Å and 2.869 to 3.449 Å for Pb−Cl and Pb−Br, respectively. The angles between Pb−X−Pb in (BZQ)Pb_2X_5 are not linear as in the case of A_2PbX_4 and are close to 90°. BZQ^+ cations form 2D arrays of orthogonally packed BZQ^+ dimers, corresponding to two parallel molecules with head-to-tail configuration. In this hybrid structure, the rigid lead halide inorganic layers provide a restricted and well-ordered environment for organic cations, improving their optical properties and thermal stability. The powder XRD patterns of (BZQ)Pb_2X_5 agrees with the simulated results obtained from the SCXRD analysis (Figure S3), indicating high phase purity of the materials. The thermal stability of these hybrid materials and their corresponding organic salts were evaluated using thermogravimetric analysis (TGA). TGA results show that (BZQ)Cl and (BZQ)Br salts decompose completely between 114 and 203 °C and between 135 and 234 °C, respectively. In the case of (BZQ)Pb_2X_5, the TGA traces show two weight loss peaks around 206 and 608 °C for $(C_{13}NH_{10})Pb_2Cl_5$ and at 262 and 572 °C for $(C_{13}NH_{10})Pb_2Br_5$, respectively (Figure S4). The first weight loss peaks correspond to the loss of BZQ^+ cations from the structures and occur at higher temperatures as compared to (BZQ)X salts. These results show that the thermal stability of BZQ^+ cations is improved in (BZQ)Pb_2X_5. In addition, (BZQ)Pb_2X_5 single crystals were found to exhibit remarkable environmental stability, with little to no change of their properties after storage in ambient conditions for a year, while the crystals of organic salts decomposed within a few days (Figures S5 and S6).

The photophysical properties of (BZQ)Pb_2X_5 (X = Cl, Br) single crystals and (BZQ)X organic salts are characterized with results shown in Figure 2 and summarized in Table 1. (BZQ)Pb_2Cl_5 and (BZQ)Cl exhibit broad featureless emissions peaked at 450 and 470 nm, respectively. The decay lifetimes of these emissions are in the nanosecond regime. The similarity between the two emissions suggests that BZQ^+ cations contribute to the emission of (BZQ)Pb_2Cl_5. By changing the halide from Cl to Br, the organic salt (BZQ)Br becomes nonemissive, while (BZQ)Pb_2Br_5 exhibits yellow emission with a microsecond decay lifetime. The emission spectrum of (BZQ)Pb_2Br_5 is broad and shows vibrational features. These results clearly suggest that the introduction of heavy atom Br influences the emission and decay lifetime of BZQ^+ cations by changing their emission character from fluorescence to phosphorescence, as it promotes spin−orbit coupling (SOC) and facilitates the intersystem crossing (ISC) from singlet to triplet state of BZQ^+ cations. The small peaks at 461 and 495 nm in the emission spectrum of (BZQ)Pb_2Br_5 are likely related to the weak emission from the singlet state, although the decay lifetime could not be recorded due to its low intensity. The emission of BZQ^+ cations is mainly attributed to (π, π^*) electronic transition similar to what has been previously reported for other BZQ salts (e.g., benzoquinolinium trifluoroacetate and benzoquinolinium trichloroacetate).[45] (BZQ)Pb_2Br_5 exhibits emission mainly from the triplet state $^3(\pi, \pi^*)$ with some contribution from the singlet state $^1(\pi, \pi^*)$, while (BZQ)Pb_2Cl_5 and (BZQ)Cl display emissions only from the singlet state $^1(\pi, \pi^*)$. The Commission Internationale de L'Eclairage (CIE) chromaticity coordinates of (BZQ)Cl, (BZQ)Pb_2Cl_5, and (BZQ)Pb_2Br_5 are (0.1603, 0.1440), (0.1675, 0.2632), and (0.3747, 0.4303),

https://doi.org/10.1021/acs.jpclett.1c02354
J. Phys. Chem. Lett. 2021, 12, 8229−8236

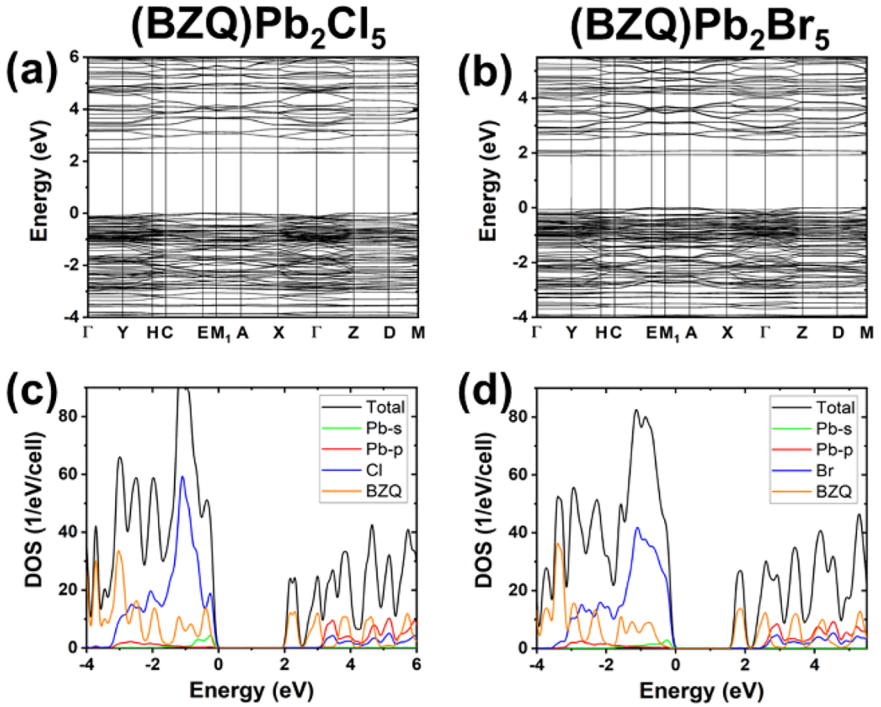

Figure 4. Electronic band structure of (a) $(BZQ)Pb_2Cl_5$ and (b) $(BZQ)Pb_2Br_5$. Density of states (DOS) of (c) $(BZQ)Pb_2Cl_5$ and (d) $(BZQ)Pb_2Br_5$ calculated using the PBE functional. Note that the PBE band gap is underestimated.

respectively (Figure 2d). The PLQE of $(BZQ)Pb_2Cl_5$ single crystals was measured at 18%, more than double that of (BZQ)Cl crystals (8%) and is attributed to decreased nonradiative decays as well as increased radiative decays. The rigid 2D $Pb_2Cl_5^-$ layers scaffold BZQ^+ cations and assist in suppressing the nonradiative relaxations of these molecules, resulting in a higher PLQE. The PLQE of $(BZQ)Pb_2Br_5$ RTP was measured at 2%, while (BZQ)Br is not emissive at room temperature. These results suggest that 2D $Pb_2Br_5^-$ layers affect the optical properties of BZQ^+ cations, not only by introducing heavy atom effects but also by providing a rigid environment for these cations. The effects of 2D $Pb_2Br_5^-$ layers on the emission of BZQ^+ cations are also displayed by the vibrational features at room temperature, which suggests more restricted cation movements.[46] The structure rigidity introduced by the inorganic layers in these hybrid materials restricts the movement of BZQ^+ cations and helps suppress the nonradiative decays, leading to enhanced emission.

The photophysical properties of these materials were also investigated at 77 K, with results showing in Figure 3 and summarized in Table 1. (BZQ)Cl exhibits blue emission with greenish-yellow afterglow upon removing the excitation source, while $(BZQ)Pb_2Cl_5$ exhibits white emission with strong yellow afterglow. The white emission of $(BZQ)Pb_2Cl_5$ at 77 K has CIE coordinates of (0.2769, 0.3408), a color rendering index (CRI) of 75, and a correlated color temperature (CCT) of 8399 K. The emission spectrum of (BZQ)Cl shows a strong peak at 445 nm with shoulders at 512 and 540 nm, while $(BZQ)Pb_2Cl_5$ displays two peaks with vibrational features and similar intensities. The decay lifetimes of the emissions in (BZQ)Cl and $(BZQ)Pb_2Cl_5$ measured at 450 nm were 8.8 and 7.53 ns, respectively. The ns character of these decay lifetimes suggests that the emissions at 450 nm correspond to fluorescence from the singlet state. The decay lifetimes monitored at 530 nm were longer and in milliseconds, indicating the phosphorescent character of these emissions. The phosphorescent decay lifetimes of (BZQ)Cl (120 ms) and $(BZQ)Pb_2Cl_5$ (150 ms) are longer than the eye detection limit (100 ms), which justifies the afterglow properties of these materials.[47] Simultaneous emissions from singlet and triplet states in $(BZQ)Pb_2Cl_5$ afford a white emission. It was previously reported that benzo[*h*]quinoline molecules can exhibit phosphorescence at rigid media and low temperatures.[48] Here, the higher rigidity provided by 2D $Pb_2Cl_5^-$ layers leads to stronger phosphorescence of $(BZQ)Pb_2Cl_5$ as compared to (BZQ)Cl. In the case of (BZQ)Br and $(BZQ)Pb_2Br_5$, strong yellow emissions with no afterglow were recorded at 77 K, as a result of suspended nonradiative decays. The decay lifetimes of (BZQ)Br and $(BZQ)Pb_2Br_5$ were recorded at 0.5 and 0.53 μs, respectively (Figure S4). These much shorter decay lifetimes as compared to those of Cl-based materials are caused by the heavy atom effects of Br, which promote SOC to afford efficient phosphorescence. These results show that metal halides can affect the photophysical properties of organic cations in multiple ways, such as controlling their molecular packing and introducing heavy atom effects.

Theoretical calculations were performed to further understand the photophysical properties of these hybrid materials. Figure 4 shows the electronic band structure and DOS of $(BZQ)Pb_2X_5$ (X = Cl, Br) calculated using the PBE functional. The electronic bands derived from organic and inorganic components have small dispersions, indicating relatively localized electronic states; this is even true for the Pb−X structure that forms 1D chains. The lack of the linear −Pb−X−Pb−X− bonds (as are present in the perovskite structure) blocks the long-range coupling among Pb-6p and halogen p orbitals in $(BZQ)Pb_2X_5$ (X = Cl, Br). The PBE band gaps of $(BZQ)Pb_2X_5$ (X = Cl, Br) are 2.31 and 1.89 eV, respectively, as shown in Figure 4. Since a PBE band gap is typically

https://doi.org/10.1021/acs.jpclett.1c02354
J. Phys. Chem. Lett. 2021, 12, 8229−8236

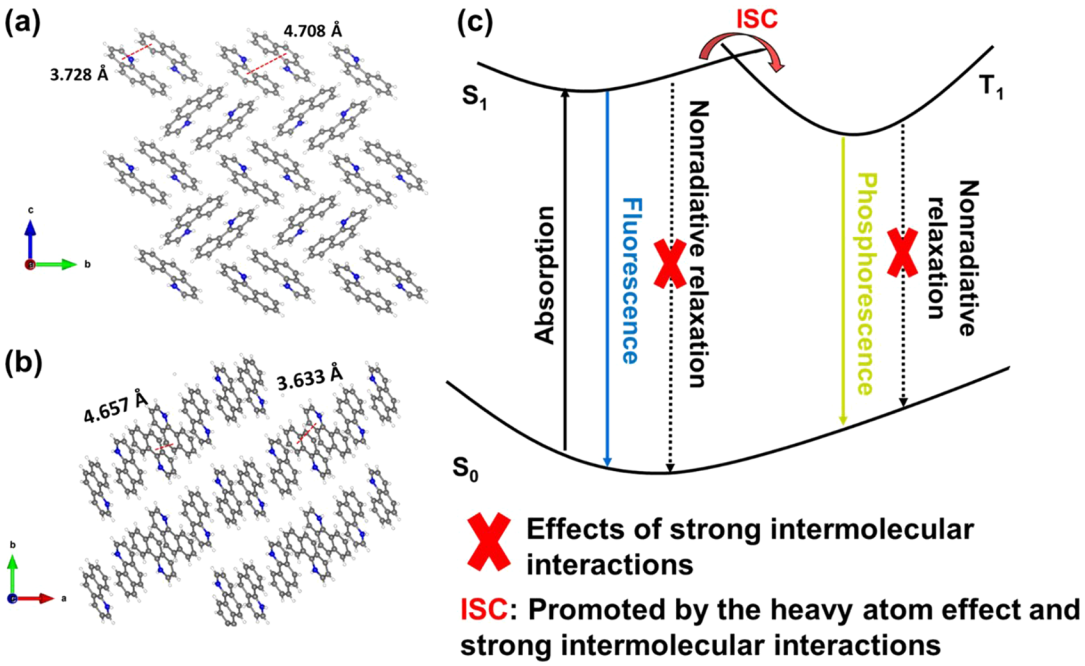

Figure 5. Molecular packing of the BZQ^+ cations in (a) $(BZQ)Pb_2Cl_5$ and (b) (BZQ)Cl. (c) Emission mechanism in $(BZQ)Pb_2X_5$.

underestimated, we further used the hybrid PBE0 calculations to correct the band gaps of $(BZQ)Pb_2X_5$ (X = Cl, Br) to 4.07 and 3.65 eV, respectively. The DOS plots in Figure 4 show that, for both compounds, the conduction band is made up of localized states from BZQ^+ cations, while the valence band is a mixing of orbitals from both inorganic and organic components. The hybridization between Pb-6s and halogen-p orbitals pushes their antibonding states to the top of the valence band. The optical excitation is most efficient when taking place locally within a BZQ^+ cation or a $Pb_2X_5^-$ layer. A close inspection of the DOS plots in Figure 4 shows that the single-party energy gap of BZQ^+ is smaller than that of $Pb_2X_5^-$ in $(BZQ)Pb_2X_5$ (X = Cl, Br). After the bandgap correction by PBE0 calculations, in $(BZQ)Pb_2Cl_5$, the single-party energy gap of BZQ^+ is about 4.1 eV, much smaller than that of $Pb_2Cl_5^-$ (5.0 eV); the corresponding energy gaps for BZQ^+ and $Pb_2Br_5^-$ in $(BZQ)Pb_2Br_5$ are about 4.0 and 4.4 eV, respectively. These results suggest that the optical emission should originate from the exciton recombination in BZQ^+ cations, which correlate well with the experimental results. The measured emission energy should be lower than the calculated energy gap due to the strong exciton binding.

To better understand the effects of molecular packing on the optical properties and thermal stability of the materials, single crystal structures of the salts (BZQ)X were determined and compared to those of $(BZQ)Pb_2X_5$ (X = Cl, Br). (BZQ)Cl and (BZQ)Br crystallize in a monoclinic system with the space group $P2_1/c$. Parts a and b of Figure 5 display the view of an array of BZQ^+ cations in $(BZQ)Pb_2Cl_5$ and (BZQ)Cl, respectively. In $(BZQ)Pb_2Cl_5$, the BZQ^+ cations form dimers with head-to-tail configurations, which pack orthogonally to form 2D arrays of cations confined by 2D $Pb_2Cl_5^-$ layers from both sides. However, in (BZQ)Cl, BZQ^+ cations form layers of linearly packed head-to-tail molecules. The intermolecular distances between the centroids of phenyl and pyridine rings range from 3.728 to 4.708 Å in $(BZQ)Pb_2Cl_5$ and from 3.633 to 4.657 Å in (BZQ)Cl, suggesting little-to-no $\pi-\pi$ interactions. C−H···Cl and N−H···Cl distances are measured between 2.147 and 2.865 Å in (BZQ)Cl and 2.343 and 2.773 Å in $(BZQ)Pb_2Cl_5$. Hirschfeld surface analysis was carried to evaluate and quantify the molecular interactions in these structures (Figure S8−S11). The 2D fingerprint plots to the Hirschfeld surface show that H···Cl interactions are stronger in $(BZQ)Pb_2Cl_5$ (31.4%) compared with (BZQ)Cl (19.4%). The molecular interactions in (BZQ)Cl were dominated by H···H interactions (62.3%), while H···Cl interactions were the most dominant interactions in $(BZQ)Pb_2Cl_5$, followed by C···H interactions. A similar comparison was observed in the case of (BZQ)Br and $(BZQ)Pb_2Br_5$. These analyses confirm that the 2D $Pb_2X_5^-$ layers scaffold and provide a rigid environment to BZQ^+ cations arrays by strong hydrogen bonding, which leads to improved thermal and environmental stability and superior optical properties in $(BZQ)Pb_2X_5$ as compared to (BZQ)X.

The proposed mechanism of the photophysical processes in $(BZQ)Pb_2X_5$ is shown in Figure 5c. $(BZQ)Pb_2X_5$ crystals are excited from a singlet ground state (S_0) to a singlet excited state (S_1). In the case of $(BZQ)Pb_2Cl_5$, fluorescence emission with ns decay lifetime occurs from the radiative relaxation of excited BZQ^+ molecules. The enhancement in BZQ^+ fluorescence in $(BZQ)Pb_2Cl_5$ as compared to (BZQ)Cl is correlated with suppression in the nonradiative decays and an increase in the structure's rigidity. The presence of Br in $(BZQ)Pb_2Br_5$, introduces heavy atom effects which promote the ISC from the singlet to triplet state (T_1). The radiative deactivation of T_1 leads to RTP with a microsecond lifetime from BZQ^+ in $(BZQ)Pb_2Br_5$.

In conclusion, organic metal halide hybrids with general formula $(BZQ)Pb_2X_5$ (X = Cl, Br) have been synthesized and characterized. The anionic metal halides ($Pb_2X_5^-$) form a unique face-sharing 2D layered structure, which acts as a scaffold for the assemblies of BZQ^+ cations and influences their photophysical properties and environmental stability. A PLQE of 18% is recorded for the fluorescence from BZQ^+ cations in $(BZQ)Pb_2Cl_5$, more than double that of (BZQ)Cl. Replacing Cl with the heavy atom Br promotes intersystem crossing effect, resulting in visible room temperature phosphorescence

https://doi.org/10.1021/acs.jpclett.1c02354
J. Phys. Chem. Lett. 2021, 12, 8229−8236

from BZQ^+ cations in $(BZQ)Pb_2Br_5$. This work paves a new way for manipulating the properties of solid-state organic chromophores via the formation of ionically bonded organic metal halide hybrid systems.

■ ASSOCIATED CONTENT

Supporting Information

The Supporting Information is available free of charge at https://pubs.acs.org/doi/10.1021/acs.jpclett.1c02354.

Experimental details, crystallographic and TGA data for all materials, PXRD data for $(BZQ)Pb_2Cl_5$ and $(BZQ)Pb_2Br_5$, emission decay curves at 77 K, and the Hiershfeld analysis (PDF)

■ AUTHOR INFORMATION

Corresponding Author

Biwu Ma − *Department of Chemistry and Biochemistry and Materials Science and Engineering Program, Florida State University, Tallahassee, Florida 32306, United States;* orcid.org/0000-0003-1573-8019; Email: bma@fsu.edu

Authors

Maya Chaaban − *Department of Chemistry and Biochemistry, Florida State University, Tallahassee, Florida 32306, United States;* orcid.org/0000-0001-8624-4409

Azza Ben-Akacha − *Department of Chemistry and Biochemistry, Florida State University, Tallahassee, Florida 32306, United States*

Michael Worku − *Materials Science and Engineering Program, Florida State University, Tallahassee, Florida 32306, United States;* orcid.org/0000-0002-0671-8588

Sujin Lee − *Department of Chemistry and Biochemistry, Florida State University, Tallahassee, Florida 32306, United States*

Jennifer Neu − *National High Magnetic Field Laboratory, Florida State University, Tallahassee, Florida 32310, United States;* orcid.org/0000-0003-4392-349X

Xinsong Lin − *Department of Chemistry and Biochemistry, Florida State University, Tallahassee, Florida 32306, United States;* orcid.org/0000-0002-0605-3029

J. S. Raaj Vellore Winfred − *Department of Chemistry and Biochemistry, Florida State University, Tallahassee, Florida 32306, United States*

Cordell J. Delzer − *Department of Nuclear Engineering, University of Tennessee, Knoxville, Tennessee 37996, United States*

Jason P. Hayward − *Department of Nuclear Engineering, University of Tennessee, Knoxville, Tennessee 37996, United States*

Mao-Hua Du − *Materials Science & Technology Division, Oak Ridge National Laboratory, Oak Ridge, Tennessee 37831, United States;* orcid.org/0000-0001-8796-167X

Theo Siegrist − *National High Magnetic Field Laboratory, Florida State University, Tallahassee, Florida 32310, United States; Department of Chemical and Biomedical Engineering, FAMU-FSU College of Engineering, Tallahassee, Florida 32310, United States*

Complete contact information is available at: https://pubs.acs.org/10.1021/acs.jpclett.1c02354

Author Contributions

M.C. and B.M. conceived the experiments and interpreted the data. M.C. synthesized and purified the materials with the help of A.B.-A.. and S.L.; M.C. collected the powder XRD data, S.L. collected the TGA data; M.C., A.B.-A., M.W. and J.S.R.V.W. measured the photophysical properties; M.C., J.N., and X.L. performed single crystal XRD analysis. C.J.D., J.P.H., and M.-H.D. performed the theoretical calculations. The manuscript was mainly written by B.M. and M.C., and revised by T.S. and M.-H.D. The project was planned, directed, and supervised by B.M. All authors discussed the results and commented on the manuscript.

Notes

The authors declare no competing financial interest.

CCDC 2092022−2092025 contain the supplementary crystallographic data for this paper. These data can be obtained free of charge via www.ccdc.cam.ac.uk/data_request/cif, or by emailing data_request@ccdc.cam.ac.uk, or by contacting The Cambridge Crystallographic Data Centre, 12 Union Road, Cambridge CB2 1EZ, UK; fax: + 44 1223 336033.

■ ACKNOWLEDGMENTS

This work was supported by the Air Force Office of Scientific Research under Contract No. FA9550-18-1-0231 and the Florida State University Office of Research. This work made use of the Rigaku Synergy-S single-crystal X-ray diffractometer acquired through the NSF MRI program (Award CHE-1828362) and the Edinburgh Instruments LP980-KS transient absorption system acquired through the NSF MRI program (Grant No. CHE-1531629). A portion of the work was conducted in the FSU Department of Chemistry & Biochemistry's MAC (FSU075000MAC) and X-ray (FSU075000XRAY) Laboratories. The theoretical calculations are based upon work supported by the Department of Energy Office of Science, Basic Energy Sciences, Materials Sciences and Engineering Division (M.-H.D.), and National Nuclear Security Administration through the Nuclear Science and Security Consortium under Award Number DE-NA0003180 (C.J.D. and J.P.H.).

■ REFERENCES

(1) Yao, X.; Li, T.; Wang, J.; Ma, X.; Tian, H. Recent Progress in Photoswitchable Supramolecular Self-Assembling Systems. *Adv. Opt. Mater.* **2016**, *4* (9), 1322−1349.

(2) Zang, L.; Che, Y.; Moore, J. S. One-Dimensional Self-Assembly of Planar π-Conjugated Molecules: Adaptable Building Blocks for Organic Nanodevices. *Acc. Chem. Res.* **2008**, *41* (12), 1596−1608.

(3) Zhao, G.; Dong, H.; Liao, Q.; Jiang, J.; Luo, Y.; Fu, H.; Hu, W. Organic field-effect optical waveguides. *Nat. Commun.* **2018**, *9* (1), 4790.

(4) Zou, S.-J.; Shen, Y.; Xie, F.-M.; Chen, J.-D.; Li, Y.-Q.; Tang, J.-X. Recent advances in organic light-emitting diodes: toward smart lighting and displays. *Mater. Chem. Front.* **2020**, *4* (3), 788−820.

(5) Desiraju, G. R. Crystal Engineering: From Molecule to Crystal. *J. Am. Chem. Soc.* **2013**, *135* (27), 9952−9967.

(6) Wang, C.; Li, Z. Molecular conformation and packing: their critical roles in the emission performance of mechanochromic fluorescence materials. *Mater. Chem. Front.* **2017**, *1* (11), 2174−2194.

(7) Guo, Y.; Xu, L.; Liu, H.; Li, Y.; Che, C.-M.; Li, Y. Self-Assembly of Functional Molecules into 1D Crystalline Nanostructures. *Adv. Mater.* **2015**, *27* (6), 985−1013.

(8) Zhang, Y.; Miao, Y.; Song, X.; Gao, Y.; Zhang, Z.; Ye, K.; Wang, Y. Single-Molecule-based White-Light Emissive Organic Solids with Molecular-Packing-Dependent Thermally Activated Delayed Fluorescence. *J. Phys. Chem. Lett.* **2017**, *8* (19), 4808−4813.

(9) Lu, B.; Liu, S.; Yan, D. Recent advances in photofunctional polymorphs of molecular materials. *Chin. Chem. Lett.* **2019**, *30* (11), 1908−1922.
(10) Lu, B.; Fang, X.; Yan, D. Luminescent Polymorphic Co-crystals: A Promising Way to the Diversity of Molecular Assembly, Fluorescence Polarization, and Optical Waveguide. *ACS Appl. Mater. Interfaces* **2020**, *12* (28), 31940−31951.
(11) Yang, J.; Zhen, X.; Wang, B.; Gao, X.; Ren, Z.; Wang, J.; Xie, Y.; Li, J.; Peng, Q.; Pu, K.; Li, Z. The influence of the molecular packing on the room temperature phosphorescence of purely organic luminogens. *Nat. Commun.* **2018**, *9* (1), 840.
(12) Nidhankar, A. D.; Goudappagouda; Mohana Kumari, D. S.; Chaubey, S. K.; Nayak, R.; Gonnade, R. G.; Kumar, G. V. P.; Krishnan, R.; Babu, S. S. Self-Assembled Helical Arrays for the Stabilization of the Triplet State. *Angew. Chem., Int. Ed.* **2020**, *59* (31), 13079−13085.
(13) Zhang, T.; Gao, H.; Lv, A.; Wang, Z.; Gong, Y.; Ding, D.; Ma, H.; Zhang, Y.; Yuan, W. Z. Hydrogen bonding boosted the persistent room temperature phosphorescence of pure organic compounds for multiple applications. *J. Mater. Chem. C* **2019**, *7* (29), 9095−9101.
(14) Liang, X.; Liu, T.-T.; Yan, Z.-P.; Zhou, Y.; Su, J.; Luo, X.-F.; Wu, Z.-G.; Wang, Y.; Zheng, Y.-X.; Zuo, J.-L. Organic Room-Temperature Phosphorescence with Strong Circularly Polarized Luminescence Based on Paracyclophanes. *Angew. Chem., Int. Ed.* **2019**, *58* (48), 17220−17225.
(15) Zhou, C.; Lin, H.; He, Q.; Xu, L.; Worku, M.; Chaaban, M.; Lee, S.; Shi, X.; Du, M.-H.; Ma, B. Low dimensional metal halide perovskites and hybrids. *Mater. Sci. Eng., R* **2019**, *137*, 38−65.
(16) Shi, E.; Gao, Y.; Finkenauer, B. P.; Akriti, A.; Coffey, A. H.; Dou, L. Two-dimensional halide perovskite nanomaterials and heterostructures. *Chem. Soc. Rev.* **2018**, *47* (16), 6046−6072.
(17) Zhou, C.; Lin, H.; Lee, S.; Chaaban, M.; Ma, B. Organic−inorganic metal halide hybrids beyond perovskites. *Mater. Res. Lett.* **2018**, *6* (10), 552−569.
(18) Li, M.; Xia, Z. Recent progress of zero-dimensional luminescent metal halides. *Chem. Soc. Rev.* **2021**, *50* (4), 2626−2662.
(19) Mao, L.; Stoumpos, C. C.; Kanatzidis, M. G. Two-Dimensional Hybrid Halide Perovskites: Principles and Promises. *J. Am. Chem. Soc.* **2019**, *141* (3), 1171−1190.
(20) Zhou, C.; Lee, S.; Lin, H.; Neu, J.; Chaaban, M.; Xu, L.-J.; Arcidiacono, A.; He, Q.; Worku, M.; Ledbetter, L.; Lin, X.; Schlueter, J. A.; Siegrist, T.; Ma, B. Bulk Assembly of Multicomponent Zero-Dimensional Metal Halides with Dual Emission. *ACS Mater. Lett.* **2020**, *2* (4), 376−380.
(21) Lee, S.; Zhou, C.; Neu, J.; Beery, D.; Arcidiacono, A.; Chaaban, M.; Lin, H.; Gaiser, A.; Chen, B.; Albrecht-Schmitt, T. E.; Siegrist, T.; Ma, B. Bulk Assemblies of Lead Bromide Trimer Clusters with Geometry-Dependent Photophysical Properties. *Chem. Mater.* **2020**, *32* (1), 374−380.
(22) Xu, L.-J.; Lin, H.; Lee, S.; Zhou, C.; Worku, M.; Chaaban, M.; He, Q.; Plaviak, A.; Lin, X.; Chen, B.; Du, M.-H.; Ma, B. 0D and 2D: The Cases of Phenylethylammonium Tin Bromide Hybrids. *Chem. Mater.* **2020**, *32* (11), 4692−4698.
(23) Zhou, C.; Lin, H.; Neu, J.; Zhou, Y.; Chaaban, M.; Lee, S.; Worku, M.; Chen, B.; Clark, R.; Cheng, W.; Guan, J.; Djurovich, P.; Zhang, D.; Lü, X.; Bullock, J.; Pak, C.; Shatruk, M.; Du, M.-H.; Siegrist, T.; Ma, B. Green Emitting Single-Crystalline Bulk Assembly of Metal Halide Clusters with Near-Unity Photoluminescence Quantum Efficiency. *ACS Energy Lett.* **2019**, *4* (7), 1579−1583.
(24) Lin, H.; Zhou, C.; Tian, Y.; Besara, T.; Neu, J.; Siegrist, T.; Zhou, Y.; Bullock, J.; Schanze, K. S.; Ming, W.; Du, M.-H.; Ma, B. Bulk assembly of organic metal halide nanotubes. *Chem. Sci.* **2017**, *8* (12), 8400−8404.
(25) Yuan, Z.; Zhou, C.; Tian, Y.; Shu, Y.; Messier, J.; Wang, J. C.; van de Burgt, L. J.; Kountouriotis, K.; Xin, Y.; Holt, E.; Schanze, K.; Clark, R.; Siegrist, T.; Ma, B. One-dimensional organic lead halide perovskites with efficient bluish white-light emission. *Nat. Commun.* **2017**, *8* (1), 14051.
(26) Lin, H.; Zhou, C.; Tian, Y.; Siegrist, T.; Ma, B. Low-Dimensional Organometal Halide Perovskites. *ACS Energy Lett.* **2018**, *3* (1), 54−62.
(27) Lin, H.; Zhou, C.; Chaaban, M.; Xu, L.-J.; Zhou, Y.; Neu, J.; Worku, M.; Berkwits, E.; He, Q.; Lee, S.; Lin, X.; Siegrist, T.; Du, M.-H.; Ma, B. Bulk Assembly of Zero-Dimensional Organic Lead Bromide Hybrid with Efficient Blue Emission. *ACS Mater. Lett.* **2019**, *1* (6), 594−598.
(28) Morad, V.; Shynkarenko, Y.; Yakunin, S.; Brumberg, A.; Schaller, R. D.; Kovalenko, M. V. Disphenoidal Zero-Dimensional Lead, Tin, and Germanium Halides: Highly Emissive Singlet and Triplet Self-Trapped Excitons and X-ray Scintillation. *J. Am. Chem. Soc.* **2019**, *141* (25), 9764−9768.
(29) Li, M.; Zhou, J.; Zhou, G.; Molokeev, M. S.; Zhao, J.; Morad, V.; Kovalenko, M. V.; Xia, Z. Hybrid Metal Halides with Multiple Photoluminescence Centers. *Angew. Chem., Int. Ed.* **2019**, *58* (51), 18670−18675.
(30) Yang, X.; Ma, L.-F.; Yan, D. Facile synthesis of 1D organic−inorganic perovskite micro-belts with high water stability for sensing and photonic applications. *Chem. Sci.* **2019**, *10* (17), 4567−4572.
(31) Zhao, J.-Q.; Jing, C.-Q.; Wu, J.-H.; Zhang, W.-F.; Feng, L.-J.; Yue, C.-Y.; Lei, X.-W. Systematic Approach of One-Dimensional Lead Perovskites with Face-Sharing Connectivity to Realize Efficient and Tunable Broadband Light Emission. *J. Phys. Chem. C* **2021**, *125* (20), 10850−10859.
(32) Zhao, J.-Q.; Sun, C.; Yue, M.; Meng, Y.; Zhao, X.-M.; Zeng, L.-R.; Chen, G.; Yue, C.-Y.; Lei, X.-W. Lead chlorine cluster assembled one-dimensional halide with highly efficient broadband white-light emission. *Chem. Commun.* **2021**, *57* (10), 1218−1221.
(33) Jing, C.-Q.; Wang, J.; Zhao, H.-F.; Chu, W.-X.; Yuan, Y.; Wang, Z.; Han, M.-F.; Xu, T.; Zhao, J.-Q.; Lei, X.-W. Improving Broadband White-Light Emission Performances of 2D Perovskites by Subtly Regulating Organic Cations. *Chem. - Eur. J.* **2020**, *26* (45), 10307−10313.
(34) Sun, C.; Guo, Y.-H.; Han, S.-S.; Li, J.-Z.; Jiang, K.; Dong, L.-F.; Liu, Q.-L.; Yue, C.-Y.; Lei, X.-W. Three-Dimensional Cuprous Lead Bromide Framework with Highly Efficient and Stable Blue Photoluminescence Emission. *Angew. Chem., Int. Ed.* **2020**, *59* (38), 16465−16469.
(35) McCall, K. M.; Morad, V.; Benin, B. M.; Kovalenko, M. V. Efficient Lone-Pair-Driven Luminescence: Structure−Property Relationships in Emissive $5s^2$ Metal Halides. *ACS Mater. Lett.* **2020**, *2* (9), 1218−1232.
(36) Smith, M. D.; Connor, B. A.; Karunadasa, H. I. Tuning the Luminescence of Layered Halide Perovskites. *Chem. Rev.* **2019**, *119* (5), 3104−3139.
(37) Han, D.; Shi, H.; Ming, W.; Zhou, C.; Ma, B.; Saparov, B.; Ma, Y.-Z.; Chen, S.; Du, M.-H. Unraveling luminescence mechanisms in zero-dimensional halide perovskites. *J. Mater. Chem. C* **2018**, *6* (24), 6398−6405.
(38) Sun, X.-Y.; Yue, M.; Jiang, Y.-X.; Zhao, C.-H.; Liao, Y.-Y.; Lei, X.-W.; Yue, C.-Y. Combining Dual-Light Emissions to Achieve Efficient Broadband Yellowish-Green Luminescence in One-Dimensional Hybrid Lead Halides. *Inorg. Chem.* **2021**, *60* (3), 1491−1498.
(39) Fattal, H.; Creason, T. D.; Delzer, C. J.; Yangui, A.; Hayward, J. P.; Ross, B. J.; Du, M.-H.; Glatzhofer, D. T.; Saparov, B. Zero-Dimensional Hybrid Organic−Inorganic Indium Bromide with Blue Emission. *Inorg. Chem.* **2021**, *60* (2), 1045−1054.
(40) Su, B.; Song, G.; Molokeev, M. S.; Golovnev, N. N.; Lesnikov, M. K.; Lin, Z.; Xia, Z. Role of Metal−Chloride Anions in Photoluminescence Regulations for Hybrid Metal Halides. *J. Phys. Chem. Lett.* **2021**, *12* (7), 1918−1925.
(41) Li, Z.; Song, G.; Li, Y.; Wang, L.; Zhou, T.; Lin, Z.; Xie, R.-J. Realizing Tunable White Light Emission in Lead-Free Indium(III) Bromine Hybrid Single Crystals through Antimony(III) Cation Doping. *J. Phys. Chem. Lett.* **2020**, *11* (23), 10164−10172.
(42) Xu, L.-J.; Plaviak, A.; Lin, X.; Worku, M.; He, Q.; Chaaban, M.; Kim, B. J.; Ma, B. Metal Halide Regulated Photophysical Tuning of Zero-Dimensional Organic Metal Halide Hybrids: From Efficient

https://doi.org/10.1021/acs.jpclett.1c02354
J. Phys. Chem. Lett. 2021, 12, 8229−8236

Phosphorescence to Ultralong Afterglow. *Angew. Chem., Int. Ed.* **2020**, *59* (51), 23067−23071.
(43) Mitzi, D. B. A Layered Solution Crystal Growth Technique and the Crystal Structure of $(C_6H_5C_2H_4NH_3)_2PbCl_4$. *J. Solid State Chem.* **1999**, *145* (2), 694−704.
(44) Shibuya, K.; Koshimizu, M.; Nishikido, F.; Saito, H.; Kishimoto, S. Poly[bis(phenethylammonium) [dibromidoplumbate-(II)]-di-[μ]-bromido]]. *Acta Crystallogr., Sect. E: Struct. Rep. Online* **2009**, *65* (11), m1323−m1324.
(45) Tervola, E.; Truong, K.-N.; Ward, J. S.; Priimagi, A.; Rissanen, K. Fluorescence enhancement of quinolines by protonation. *RSC Adv.* **2020**, *10* (49), 29385−29393.
(46) Orrit, M.; Bernard, J.; Personov, R. I. High-resolution spectroscopy of organic molecules in solids: from fluorescence line narrowing and hole burning to single molecule spectroscopy. *J. Phys. Chem.* **1993**, *97* (40), 10256−10268.
(47) Xu, S.; Chen, R.; Zheng, C.; Huang, W. Excited State Modulation for Organic Afterglow: Materials and Applications. *Adv. Mater.* **2016**, *28* (45), 9920−9940.
(48) Kanda, Y.; Shimada, R. The triplet-singlet emission spectra of phenanthrene and related compounds in EPA and in petroleum ether at 90° K. *Spectrochim. Acta* **1959**, *15*, 211−224.

https://doi.org/10.1021/acs.jpclett.1c02354
J. Phys. Chem. Lett. 2021, 12, 8229−8236